Nanoscale Advances

Accepted Manuscript

This article can be cited before page numbers have been issued, to do this please use: K. B. Tummaluru, F. A. Inam and J. M. Laskar, *Nanoscale Adv.*, 2026, DOI: 10.1039/D6NA00100A.

ROYAL SOCIETY OF CHEMISTRY

rsc.li/nanoscale-advances

View Article Online
DOI: 10.1039/D6NA00100A

A comprehensive design framework for all-dielectric metasurfaces by harnessing the interplay of controlled multiple multipoles excitation, Rayleigh anomaly, Mie and lattice resonances

Tummaluru Khadar Basha,[1] Faraz A. Inam,[2] and Junaid Masud Laskar[1]*,
Nanophotonics and Quantum Meta-Optics Group, Center for Nanophotonics, Department of Physics and Nanotechnology, Kattankulathur, Chennai, Tamil Nadu, PIN- 603203, India
Department of Physics, Aligarh Muslim University, Aligarh, Uttar Pradesh, PIN-202002, India
(*Electronic mail: junaidmb@srmist.edu.in)

Abstract
Dielectric metasurfaces have emerged as promising candidates to control electromagnetic (EM) multipoles, crucial for precise manipulation of associated light-matter interactions, particularly for multifunctionality in photonics technologies spanning across structural scales and EM spectrum. Each multipole with a given nature (electric-E, magnetic-H) and order (dipole-D, quadrupole-Q) has specific functionality, having implications on resonance types- fundamental as well as collective, their coupling, and hybridization. On using geometrical dimensions as primary design parameters, only a few multipoles could be excited simultaneously. Moreover, understanding the relationship among meta-atom Mie resonance, lattice periodicity, and lattice resonances is still missing. Local field distribution due to the spatial hybridization with neighboring meta-atoms is also unknown for finite metasurfaces. We have developed a comprehensive design framework to maximize resonance strength by controlled multipoles excitation, overlap, coupling among different resonance types- Mie, lattice, Rayleigh anomaly, and local field in metasurface, using numerical simulation. Simultaneous spectral overlapping of four (ED, MD, EQ, MQ) multipoles is demonstrated as meta-atom height exceeds excitation wavelength. As periodicity matches both Mie and Rayleigh anomaly wavelength, resulting in a metasurface resonance attains a high Q-factor, attributed to maximum coupling of Mie and lattice resonances. Spatial field hybridization due to specific arrangement of neighboring meta-atoms, depending on array size, results in asymmetric local field distribution in finite metasurfaces, crucial for real-world implementation. Our findings reveal governing principles linking controlled multipole excitation dynamics, influence of coupling among different resonance types on resultant resonance, and local field distribution relevant towards multifunctional metasurface photonics integrated quantum technologies.

Keywords: finite metasurface, multipole, Rayleigh anomaly, hybridization, Mie, lattice resonance

Introduction
Resonances are ubiquitous in nature, creating striking visual effects, as in opal gemstones[1], beetles[2], butterfly wings[3], particularly in the context of light–matter interactions[4], arising in systems where an electromagnetic (EM) wave interferes with a geometry to create a strong EM field enhancement at specific frequencies or wavelengths[5]. Resonant systems span from simple geometric cavities, such as an antenna[6], meta-atom[5,7–9], Fabry–Perot[10], ring[11], whisper gallery resonators[12] to complex periodic structures- photonic crystal[13], metasurfaces[5,8,9,14–16], by making use of different mechanisms, including Mie[5,9,14–17], plasmonic[7], guided-mode[18,19], Fano resonances[20], lattice resonances[21–24], and bound states in the continuum (BICs)[25].

View Article Online
DOI: 10.1039/D6NA00100A

In the dielectric meta-atom, being a basic resonant photonic system, having their dimension of the order of the excitation EM wavelength and its match with the wavelength of EM multipole oscillation of different nature (electric and magnetic) and order (dipoles, quadrupoles), resonant excitation of multipoles takes place, known as Mie resonances (λ_{Mie}) [9,14–17,26,27]. Computational design and experimental investigation of meta-atoms of different shapes are carried out through resonant multipole excitation, amplitude enhancement, spectral tuning, and overlap of multiple resonance peaks. However, despite the significant effort in the last decade, multipole overlap has been limited to only electric multipoles of two different orders– ED, EQ, and lower-order MD, therefore, leaving out MQ, which is crucial to enhance the magnetic emitter emissivity, and nonlinear optical signals[9,14–16,26]. It still remains a challenge to simultaneously harness four multipoles of different nature and order – ED, MD, EQ, and MQ, through their overlap as well as their field enhancement to nearly equal amplitude at a fixed geometrical dimension.

A 2D crystal lattice structure, with the meta-atoms acting as the crystal basis located at the lattice sites, is known as the metasurface[5,7,15,16,28,29]. Metasurface is one of the most prominent resonant photonic systems, which allows to realize high Q-factor, a characterizing parameter of a resonator defined by the ratio of energy stored to energy lost per radiation cycle[30]. The metasurface lattice resonance (λ_{MS-Res}), manifested as peaks in the EM spectra, originates from the coupling among Mie resonances ($\lambda_{Mie} \equiv \lambda_{MA-Res}$) corresponding to each meta-atom and lattice periodicity (P_{MS}), i.e., meta-atom spacing dependent lattice resonances (λ_{LS-Res}) [7,15,16,21,22,30–33]. EM wave interaction with a periodic lattice structure, not necessarily having resonant meta-atoms as the basis, results in a diffraction pattern, which is the appearance of alternating intensity maxima and minima, also known as the lattice resonances or diffraction orders, whose angular positions can be accurately estimated by diffraction theory[34]. Interestingly, as an anomaly to the diffraction theory, rapid variations in expected intensities corresponding to different diffraction orders, known as the Rayleigh anomaly (RA) at specific wavelengths (λ_{RA}) depending on the lattice periodicity (P_{MS}), are observed in the diffraction gratings, the periodic lattice structures of both metals, as well as dielectrics[19,31,34–36]. On varying the values of the metasurface P_{MS}, around the corresponding λ_{RA} values, along two different horizontal directions of a metasurface, enhancement of lattice resonances (LR) due to combinations of two multipoles of different nature and order- (a) ED-LR[15,23,30,37], MD-LR[15,23,30,32,37,38], (b) MD-LR[15,23,30,32,37,38], EQ-LR[15,23,30,39–41], as well as due to single multipole – (a) ED-LR[30,37], (b) MQ-LR[39,42], are shown previously. However, in order to achieve an extremely high Q-factor in a metasurface, simultaneous overlap of multiple multipoles of different nature and order needs to be resonantly excited together with their spectral overlap. In this regard, a larger range of meta-atom spacing, the lattice periodicity (P_{MS}) around the corresponding λ_{RA} values need to be explored. Therefore, an investigation of the role of P_{MS} on the interplay among different natures and order of multipoles, as well as resonance types- (i) the meta-atom Mie resonance (λ_{MA-Res}), (ii) metasurface lattice resonances (λ_{MS-Res}), and (iii) Rayleigh anomaly wavelength (λ_{RA}), across a larger range of lattice periodicity (P_{MS}) spanning four regimes - (a) small ($P_{MS} < \lambda_{MA-Res}$), (b) intermediate ($P_{MS} \leq \lambda_{MA-Res}$), (c) of the order ($P_{MS} \sim \lambda_{MA-Res}$) and (d) large ($P_{MS} > \lambda_{MA-Res}$). It will provide a deeper insight.

Metasurfaces used in real-world applications are constituted by a finite number of meta-atoms. However, investigations carried out until now have been mostly focused on computational design simulations of infinite metasurfaces, in order to reduce the computational cost by modelling the unit cell only and applying periodic boundary conditions[43]. In infinite metasurface numerical

View Article Online
DOI: 10.1039/D6NA00100A

simulations, amplitude enhancement of resonantly excited EM multipoles and role of their coupling on resultant high Q-factor resonance in the EM spectra can only be computed[33,44–47]. The knowledge of local EM field distributions around specific locations of each meta-atom in the nearfield, particularly the influence of neighboring meta-atoms and their spatial arrangement, is hardly addressed in the infinite metasurface numerical computation.

In this paper, by making use of finite element method-based numerical computational simulations, we have developed a comprehensive conceptual design framework to maximize the dielectric metasurface resonances and near field distributions at sub meta-atom scale, harnessing simultaneous resonant excitation of different nature and order EM multipoles corresponding to different resonance types across the hierarchical scales. Particularly, the interplay of crucial control parameters - the meta-atom geometrical dimensions (diameter-D_{MA}, and height-H_{MA}), metasurface lattice periodicity with regard to Rayleigh anomaly wavelength (λ_{RA}) and number of meta-atoms (N_{MS}) on meta-atom Mie resonances (λ_{MA-Res}), their coupling with diffraction lattice resonances and EM field hybridization due to spatial arrangement of neighboring meta-atoms, is investigated systematically. Deeper insight into these studies is crucial for real-world metasurface applications, including Huygens metasurface[48], quantum electrodynamics-based cavity-free resonant integrated photonic devices[46], integration with quantum light sources[49], Raman emitters[50], low-threshold nano-lasers[51], and quantum sensing[52].

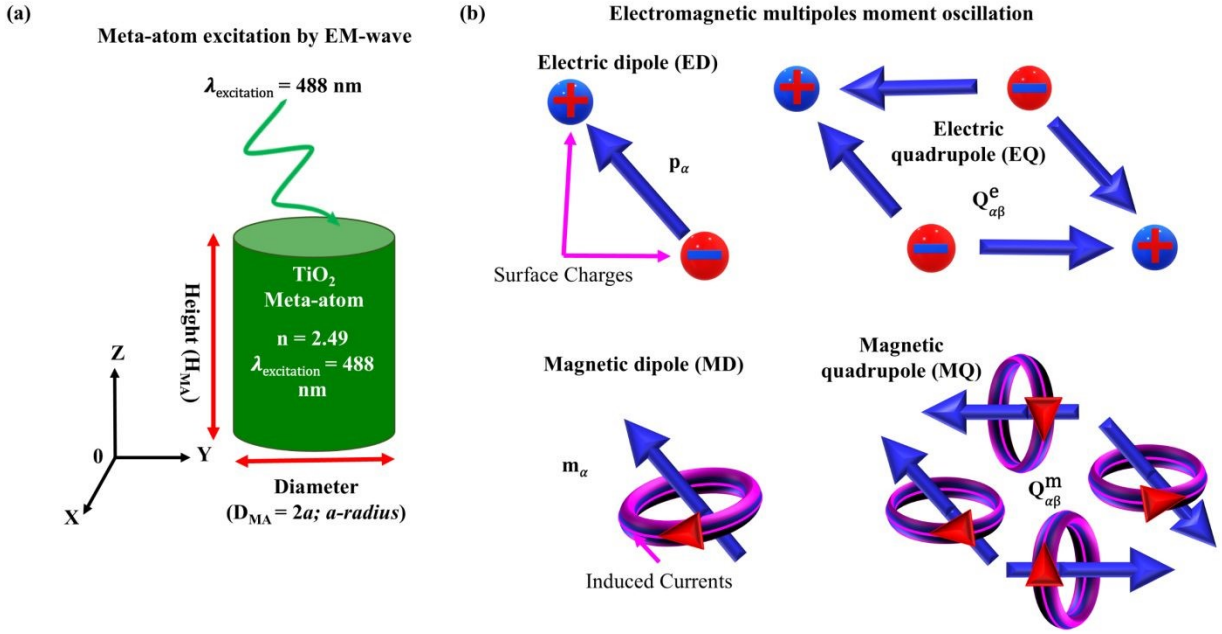

Fig. 1: a Schematic of an EM wave excitation of a meta-atom (TiO_2, $n_{TiO_2} = 2.49$ @ $\lambda_{excitation} = 488$ nm), **b** EM multipole moment dipole oscillation configurations.

Numerical computation (finite element method- FEM) of scattering cross-section (C_{sca}) and EM field distribution of both finite and infinite metasurfaces

The numerical computational simulations of EM scattering cross-sections (C_{sca}) and EM field distributions for (a) a cylindrical dielectric (TiO_2) meta-atom, (b) infinite metasurface on applying periodic boundary conditions (PBC) and (c) metasurface with finite number of meta-atoms, are performed using finite element method (FEM) – the EM wave frequency domain of wave optics module [COMSOL multiphysics software (version 6.2)]. The EM wave excitation of the meta-

View Article Online
DOI: 10.1039/D6NA00100A

atom and metasurface are done along the Z-direction (Fig. 1a), with air ($n_{air} = 1$) as the surrounding medium. Previously reported values of the refractive indices are used for both the meta-atom (TiO_2, $n_{TiO_2} = 2.49$ @ $\lambda_{excitation} = 488$ nm)[53] as well as for the substrate (Si, $n_{Si} = 3.65$ @ $\lambda_{excitation} = 488$ nm)[54]. In order to minimize undesired reflections of the scattered EM waves, a perfectly matched layer (PML), an artificial absorbing layer, is used at the interface boundary with surrounding air medium. The size of the mesh elements is varied from 2 nm to ($\lambda_{excitation}/6$) to ensure accurate computation of EM field distribution. The induced current densities ($\boldsymbol{J_\omega}$)[55] (Eq. 3 - Supplemental Information), thereby the EM multipole moments of different orders (Eqs. 4 – 7 – Supplemental Information) are computed for each element corresponding to a certain value of spatial position vector ($\boldsymbol{r}$) [Fig. 1].

Results and discussion

The role of the geometric parameters, the meta-atom height (H_{MA})**,** metasurface array periodicity (P_{Ms}), and number of meta-atoms (N_{Ms}) on the C_{sca}^{total} as well as on the scattering cross sections corresponding to multipole moments – ED, MD, EQ, MQ are investigated, particularly in the Mie regime –$H_{MA} \sim P_{Ms} \sim \lambda_{excit}$.

Height of meta-atom dictates the overlap of multiple EM multipoles- The Mie resonance

With an increase in meta-atom height (H_{MA}), a shift of the multipole peaks and their overlap in the EM spectra, are observed on excitation by the EM wave $\lambda_{excitation} = 488\,nm$), as shown in Fig. 2. The total scattering cross section (C_{sca}^{total}) is shown as a function of size parameter ($ka = \frac{2\pi na}{\lambda_{excitation}}$)[56]. The spectral peaks physically signify decomposition of Mie resonances into multipoles of different nature (electric and magnetic) and orders (dipoles and quadrupoles)[56–58]. The lower-order multipoles- ED and MD can be excited at shorter meta-atom heights ($H_{MA} < \lambda_{excitation}$) [57,58]. With an increase in height ($H_{MA} \sim \lambda_{excitation}$, Fig. 2c), the amplitude of lower-order resonance modes- ED and MD - do not vary significantly. However, their spectral peak width decreases, signifying an enhancement in the Q-factor of the corresponding mode. The meta-atoms with shorter height ($H_{MA} < \lambda_{excitation}$) [Figs. 2 (a & b)] are unable to support the higher-order multipoles- EQ and MQ[40,59].

On significantly increasing meta-atom height ($H_{MA} > \lambda_{excitation}$, Fig. 2d), two significant aspects are observed with regard to higher order multipoles (EQ and MQ)- (a) enhancement of the peak amplitude, (b) spectral peak shift towards lower size parameter values ($ka = 0.77$). This red spectral shift leads to a larger degree of overlap of higher order multiples (EQ and MQ) with the lower ones (ED and MD), both in terms of spectral peak position and amplitude [Fig. 2d][57,58]. The red shift of spectral peak as a function of increasing height (H_{MA}) is also observed for dielectric Si meta-atom, unlike the blue-shift observed for plasmonic meta-atom, attributed to increased restoring force between positively charged atomic nuclei and the displaced negatively charged electron cloud, on being excited by an EM wave[58].

View Article Online
DOI: 10.1039/D6NA00100A

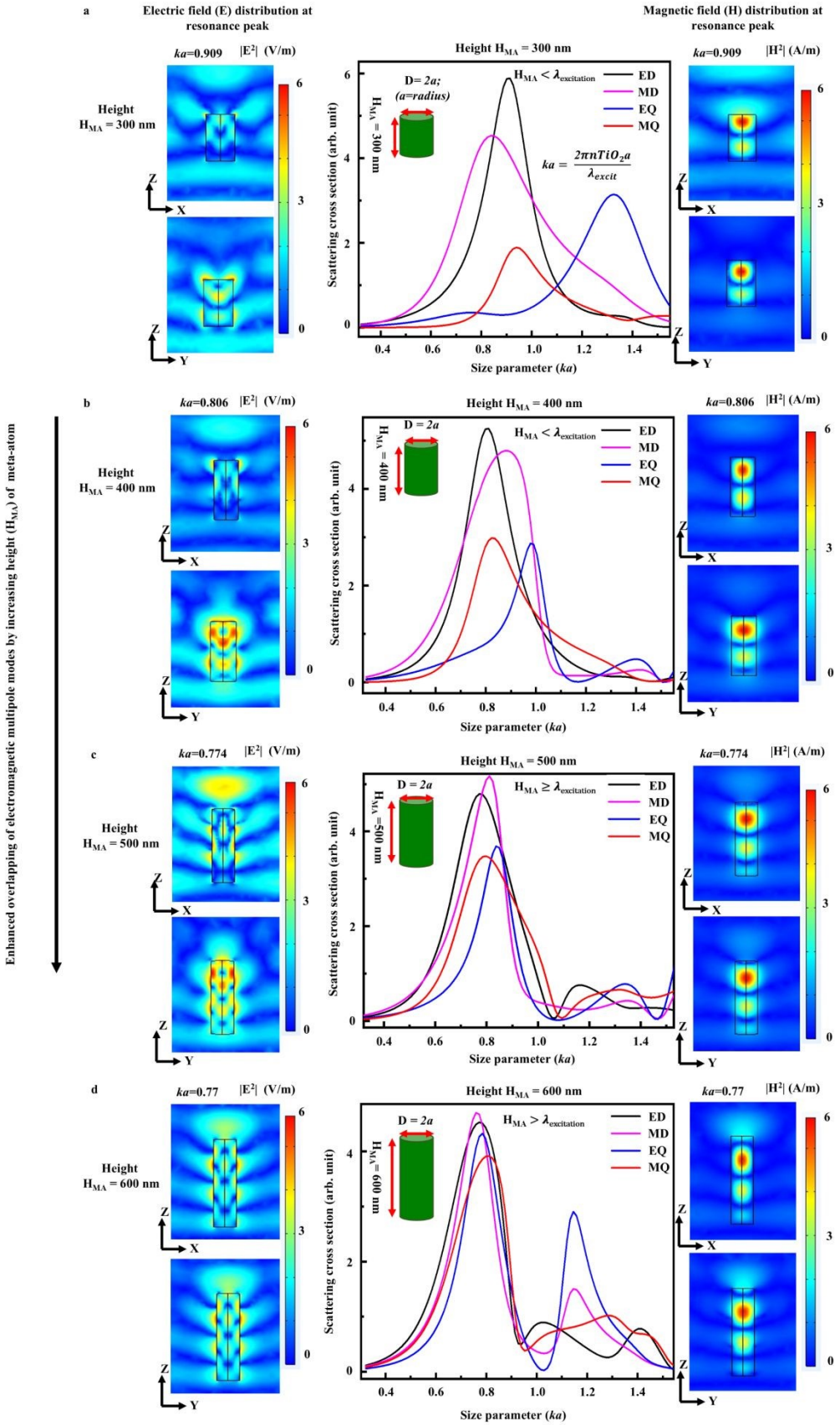

Fig. 2: Scattering cross-section (C_{sca}^{total}) of EM multipole for different meta-atom heights (H_{MA}).

View Article Online
DOI: 10.1039/D6NA00100A

Physically, the higher order multipoles in dielectrics (TiO_2, Si, etc.), particularly the quadrupole moments (EQ and MQ), can be considered as a couple of anti-parallel dipole moments [Fig. 1b], which requires sufficiently large enough physical space along a specific direction, which in this case is the Z axis- the meta-atom height H_{MA} direction, so that a quadrupolar arrangement of field distribution can be accommodated within the meta-atom[59]. Moreover, increased meta-atom height H_{MA}, having larger values of position vectors ($\boldsymbol{r}$) (Fig. 1), satisfies the condition for the Bessel functions of first kind with higher orders (second and third- j_2 and j_3) $\frac{j_1(kr)}{kr}$ together with inverse power law ($\frac{1}{r^2}$ & $\frac{1}{r^3}$), so that maxima peaks are allowed to form, acting as the higher order modes- EQ and MQ (Eqs. 4 & 5)[55]. Despite the overlap of all the multipoles (ED, MD, EQ, MQ) at size parameter *ka* = 0.77, designated as Mie mode-1, a new mode-2 also gets developed at larger *ka* = 1.2, where both enhancement and overlap of multipoles take place, for $H_{MA} > \lambda_{excitation}$, as shown in Fig. 2d. The enhancement of Mie multipole modes and their overlap signify that for a meta-atom with a given refractive index (n), the geometric parameter – the meta-atom height H_{MA} normalized with regard to the excitation wavelength $\lambda_{excitation}$ can be used as the primary control design parameter for efficient design of metasurfaces for diverse applications, including multipolar Huygens metasurface[48], directional scattering[60], superdirectivity[61].

Lattice periodicity (P_{MS}) dictates coupling among Mie and lattice resonances

Metasurface, a 2D lattice structure, is designed by placing each meta-atom, acting as the basis, at the lattice sites, as shown in Fig. 3a[62]. Unlike the Mie resonance occurring at a wavelength λ_{MA-Res} ($= 463\ nm$) corresponding to a meta-atom, interaction among each meta-atom resonance, depending on the lattice periodicity (P_{MS})**,** play a crucial role on the resulting resonance, known as metasurface lattice resonance (λ_{MS-Res}), manifested as peaks in the EM spectra[32,63]. Interaction of light with a periodic lattice structure, not necessarily having Mie resonant meta-atoms as the basis, results in an EM wave diffraction pattern, which is the appearance of alternating maxima and minima, the lattice resonances ($\lambda_{Lattice-Res}$), also known as diffraction orders in the light intensity pattern, whose angular positions can be accurately estimated by diffraction theory[19]. However, as an anomaly to the diffraction theory, rapid variations in the intensities of diffraction orders, known as the Rayleigh anomaly (RA), are observed in the diffraction gratings, periodic lattice structures of both metals, as well as dielectrics[19,36]. The variations in the appearance of intensity maxima occur at Rayleigh anomaly (RA) wavelengths (λ_{RA}), which also depends on the lattice periodicity (P_{MS}) of the diffraction grating, including a crossed grating in 2D, as in the case of metasurfaces[19,36]. The λ_{RA} for a metasurface (TiO_2) on an opaque substrate (Si), not only depends on P_{MS}, but also the effective metasurface refractive index (n_{eff})[64], (Eq. 8 Supplemental Information), as given by the expression $\lambda_{RA} = n_{eff} \times P_{MS}$ Fig. 3d.

View Article Online
DOI: 10.1039/D6NA00100A

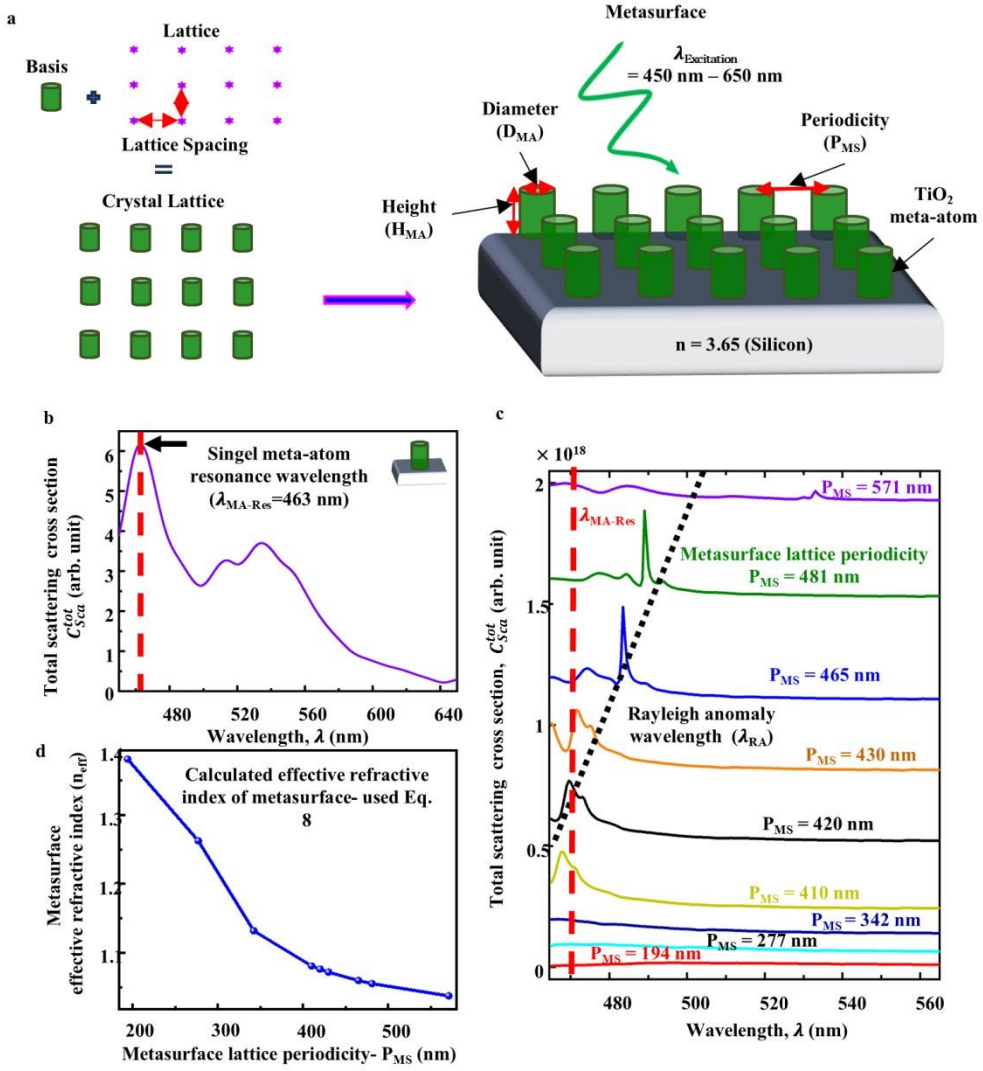

Fig. 3: **a** Schematic of a metasurface, **b** Total scattering cross-section (C_{sca}) EM spectra of a meta-atom, **c** across different metasurface lattice periodicity (P_{MS}), and **d** Calculated metasurface effective refractive index (n_{eff}).

The role of P_{MS} on the interplay among different resonance types- (i) the meta-atom Mie resonance (λ_{MA-Res})[30], (ii) metasurface lattice resonances (λ_{MS-Res})[21,63], and (iii) Rayleigh anomaly wavelength (λ_{RA})[36], across three regimes of lattice periodicity (P_{MS})- (a) small ($P_{MS} < \lambda_{MA-Res}$), (b) intermediate ($P_{MS} \leq \lambda_{MA-Res}$), (c) of the order ($P_{MS} \sim \lambda_{MA-Res}$) and (d) large ($P_{MS} > \lambda_{MA-Res}$), is investigated. The EM wave scattering cross section (C_{sca}) is computed for a TiO_2 metasurface on a Si substrate, as a function of wavelength ($\lambda = 450 - 650$ nm) for different lattice periodicity (P_{MS}) [Fig. 3c], considering the optimally designed resonant dimensions of a meta-atom in air medium, obtained by numerical computation as discussed earlier. The meta-atom resonance wavelength (λ_{MA-Res}) is found to be 463 nm for the designed TiO_2 meta-atom on a Si substrate, for the optimal dimensions ($D_{MA} = 120$ nm and $H_{MA} = 600$ nm), as shown in Fig. 3a. As the lattice periodicity (P_{MS}) is increased from $P_{MS} < \lambda_{MA-Res}$ to $P_{MS} > \lambda_{MA-Res}$, three aspects are observed with regard to the resonance peak in the spectra- (a) red-shift towards longer

View Article Online
DOI: 10.1039/D6NA00100A

wavelength, (b) narrowing of the width and (c) shift towards λ_{RA} [Figs. 3 (b & c)]. For small periodicity regime- $P_{MS} < \lambda_{MA-Res}$ ($P_{\mathrm{MS}} = 194$ nm, 222 nm, and 342 nm :$\lambda_{MA-Res} = 463$ nm), no spectral peak is observed within investigated wavelength range [Fig. 3c], as the probability of satisfying resonance conditions ($\lambda_{MS-Res} < 450$ nm) is higher at shorter wavelengths[65]. Moreover, the calculated values of λ_{RA} [Fig. 3c], being very low for small periodicity ($P_{MS} < \lambda_{MA-Res}$), do not fall within the investigated wavelength range. For intermediate periodicity regime, $P_{MS} \leq \lambda_{MA-Res}$ ($P_{MS} = 410$ nm, 420 nm, and 430 nm, $\lambda_{MA-Res} = 463$ nm), the observed spectral peaks (λ_{MS-Res}) are found to broad and lie at shorter wavelengths compared to Rayleigh anomaly wavelength(λ_{RA}), i.e. $\lambda_{MS-Res} < \lambda_{RA}$ [Fig. 3c] [21,32,37,41,66]. The metasurface lattice resonances (λ_{MS-Res}) originate from the coupling, i.e. constructive interference of far-field interactions among the meta-atom resonances (λ_{MA-Res}). However, the coupling is weak, leading to weak interference, manifested as the broad width of the observed lattice resonance spectral peaks, if the meta-atoms are close to each other in intermediate periodicity regime ($P_{MS} \leq \lambda_{MA-Res}$), as shown in Fig. 3c. Moreover, the metasurface lattice resonance λ_{MS-Res} positions are found to approach the corresponding λ_{RA} values, with increase in P_{MS}. The λ_{MS-Res} resonances are strongly coupled with ED, MD, and EQ, these modes are called as ED-LR, MD-LR, and EQ-LR (shown in Fig. S1 – Supplemental Information).

In the periodicity regime $P_{MS} \sim \lambda_{MA-Res}$ ($P_{MS} = 465$ nm, and 481 nm), the optimum spacing among the meta-atoms, the spectral peak width becomes extremely narrow, which is attributed to the collective resonance resulting from the maximum coupling between two different nature of EM resonances- λ_{MA-Res} and $\lambda_{Lattice-Res}$[21,37,40,65]. There is strong enhancement from the ED-LR, MD-LR, and MQ-LR shown in Fig. 4. Interestingly, the λ_{MS-Res} resonance spectral peak positions almost overlap with the respective λ_{RA} wavelength values [Figs. 3(b & c)]. Observation of λ_{MS-Res} either overlapping with or in the proximity of the calculated λ_{RA} (dotted line) physically means that both meta-atom Mie resonance (λ_{MA-Res}) (dashed line) and P_{MS} dependent lattice diffraction resonance makes equal contributions. Otherwise, meta-atom Mie resonance (λ_{MA-Res}) primarily plays the key role. For larger periodicity regime, $P_{MS} > \lambda_{MA-Res}$ ($P_{MS} = 571$ nm), i.e. for large separation among the meta-atoms, the spectral peak almost gets diminished only showing a tiny amplitude, signifying non-satisfying of metasurface lattice resonance condition (λ_{MS-Res}), as shown in Fig. 3c[19,40,65]. This aspect is confirmed by the significant departure of the tiny spectral peak (λ_{MS-Res}) position from the λ_{RA} value, which means the necessary crossed grating diffraction condition is not satisfied for such large values of lattice periodicity[65]. Therefore, for a given metasurface lattice structure on an opaque substrate, on using the lattice periodicity (P_{MS}) as a control parameter across different periodicity regimes, with regard to single meta-atom resonance wavelength (λ_{MA-Res}) and Rayleigh anomaly wavelength (λ_{RA}), the coupling among different nature of lattices resonances can be maximized, therefore, resulting in extremely strong metasurface lattice resonances λ_{MS-Res}, with extremely narrow width, high magnitude and large quality factor[30].

Number of meta-atoms in finite metasurface dictates spatial hybridization of EM multipoles

The computational simulations are in general performed by only modelling the unit cell of the array of meta-atoms, and applying periodic boundary conditions, thereby modelling an infinite metasurface[62]. This approach significantly reduces computational cost compared to modeling a finite array of individual meta-atoms. However, no array is infinite in real nanophotonic systems, and usually the size of the arrays that can be created is limited by the fabrication method[43].

View Article Online
DOI: 10.1039/D6NA00100A

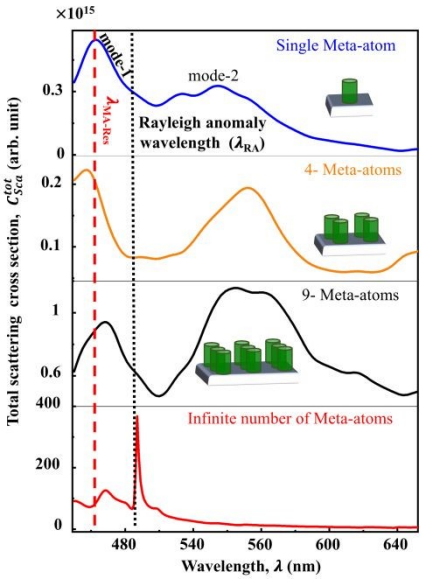

Fig. 4: Total scattering cross-section (C_{sca}) EM spectra of metasurface for different number of meta-atoms.

Considering real metasurfaces with finite lattice array size, i.e., a finite number of meta-atoms, computational simulations are compared for single, 4 (2×2), 9 (3×3) meta-atoms, and an infinite metasurface. In order to design finite metasurfaces, the optimal geometric dimensions- the meta-atom height, diameter in the periodicity regime ($P_{MS}\sim \lambda_{MA-Res}\sim 463\ nm$) are considered, where maximum resonance, manifested as sharp peak width (FWHM) and high Q-factor are observed, because of collective resonance (λ_{MS-Res}) resulting from the maximum coupling between two different nature of EM resonances- λ_{MA-Res} and $\lambda_{Lattice-Res}$, as discussed in the previous section [Fig. 3]. Although, it is speculated that the strength of the coupling, manifested as the resonance peak width, is dictated by the metasurface array size, i.e. the number of meta-atoms, a systematic investigation is still missing.

In this regard, the role of increasing number of meta-atoms (N_{MA}) on the interplay among different metasurface resonance types, λ_{MA-Res}, $\lambda_{Lattice-Res}$, λ_{RA} and λ_{MS-Res}, are examined for $P_{MS}\sim \lambda_{MA-Res}$, as shown in Fig. 4. Two distinct collective metasurface resonance modes (λ_{MS-Res})-designated as mode-1 and mode-2 are observed, on increasing number of meta-atoms (N_{MA}), while spatially arranged in a symmetric manner. In the case of a single meta-atom (Fig. 4), mode-1 ($\lambda_{MA-Res-mode-1}$) appears significantly stronger than mode-2 ($\lambda_{MA-Res-mode-2}$). In order to get a better idea about the contribution of multipole nature (electric or magnetic) and order (dipole or quadrupole) on the total scattering cross section (C_{sca}^{total}), scattering cross section for each multipole (ED, MD, EQ, MQ) is computed (Fig. S2 - Supplemental Information). All the four multipoles significantly contribute to the resultant resonance mode-1 (shown in Fig. S2 – Supplemental Information), whereas mode-2 is primarily supported by the MD and EQ, with less contributions from the ED and MQ. As per the phase symmetry of the EM multipoles, ED and MQ are of even parity, while MD and EQ are of odd parity[44,67]. Hence, the mode-2 for single meta-atom is primarily contributed by multipoles of same parity, with different nature and order. On increasing the number of meta-atoms ($N_{MS}=4\,;\ 2\times 2$), while satisfying the optimal periodicity regime condition - $P_{MS}\sim \lambda_{MA-Res}$, the amplitude of resonance mode-2 is found to become comparable to

View Article Online
DOI: 10.1039/D6NA00100A

resonance mode-1. The lower-order multipoles of different nature (ED and MD) and parity make the major contribution to mode-1. Multipoles, ED and MQ, with different nature and order, however with same parity primarily contribute to mode-2 (shown in Fig. S2 – Supplemental Information)[44,67].

On further increase in the number of meta-atoms (3×3), the amplitude of resonance mode-2 surpasses that of mode-1, as shown in Fig. 4. EM multipoles (ED, EQ and MQ) with different nature, order, and parity except MD contribute to resonance mode-1[44,67]. However, all four multipoles make equal and significant contributions to mode-2, leading to the surpassing the amplitude of mode-1. Therefore, on increasing the number of meta-atoms ($1 \rightarrow 9$), the following aspects are found to be noteworthy- (i) the resonance mode-1, the λ_{MA-Res} makes a small red shift towards λ_{RA} position, (ii) the resonance mode-2, the λ_{MS-Res}, resulting from the coupling among λ_{MA-Res} and $\lambda_{Lattice-Res}$, makes a large blue shift towards λ_{RA} position, signifying the role of lattice periodicity on collective metasurface lattice resonances (λ_{MS-Res}), with increasing number of meta-atoms[44,67]. In the case of infinite metasurface ($N_{MS} = \infty$), modeling infinite number of meta-atoms on applying periodic boundary condition as discussed in Fig. 3c, resonance mode-1 almost gets diminished, while resonance mode-2 becomes predominant, having extremely narrow width and high amplitude, indicating the emergence of a high Q-factor resonance [Figs. (3c & 5)][44,68,70]. Interestingly, the resonance mode-2 (λ_{MS-Res}) wavelength position exactly overlaps with the λ_{RA} position, if the optimal periodicity regime condition - $P_{MS} \sim \lambda_{MA-Res}$ is satisfied, for infinite metasurface. The three multipoles (ED, MD and MQ) are found to makes the major contributions in resonance mode-2, with hardly any contribution from the EQ[37,47].

Local EM field distribution is influenced by spatial hybridization of EM multipoles corresponding to neighboring meta-atoms

In addition to the knowledge of finite meta-atom metasurfaces at global scale, understanding the total scattering cross section (C_{sca}^{total}) and field distributions (electric $-|E|^2$ and magnetic $-|H|^2$) at the local meta-atom scale is crucial for different applications including quantum emitters[49], Raman signal enhancement[50], low threshold nano-lasers[51], and other cavity-free integrated resonant photonic circuit devices[52]. It is to be noted that while designing the finite metasurfaces (TiO_2 on Si substrate) with different number of meta-atoms (2×2 and 3×3), optimal geometric dimensions- the meta-atom height, diameter and lattice periodicity ($P_{MS} \sim \lambda_{MA-Res}$) are considered, where the metasurface resonances (λ_{MA-Res}), manifested as narrow spectral peak width (FWHM) with high quality (Q) factor, are observed[44,68,70].

In the case of a finite metasurface with 2×2 meta-atoms, the C_{sca}^{total}, considering multipoles (ED, MD, EQ and MQ) of different order and nature for each meta-atom (index- 1, 2, 3 and 4), are found to exactly overlap with each other, as shown in Fig. 5. Both the electric as well as magnetic field show asymmetric distribution, where the field strengths $|E|^2$ and $|H|^2$ are higher for each meta-atom in the direction of its outer periphery and not having any neighboring meta-atom, as observed in both horizontal cross-sectional (XY plane, Z= 280 nm) and vertical cross-sectional (XZ plane, Y= 232.5 and -232.5 nm) planes. The periodicity regime $P_{MS} \sim \lambda_{MA-Res}$, i.e. the separation distance between two neighboring meta-atoms (P_{MS}) is of the order of single meta-atom resonance wavelength (λ_{MA-Res}), is found to be optimal for maximum strength mode coupling with neighboring meta-atom field distribution, known as spatial hybridization, resulting strong local field in the meta-atom of interest[69–71]. This leads to the redistributing the fields of each

View Article Online
DOI: 10.1039/D6NA00100A

meta-atom towards outer periphery in the direction away from the neighboring meta-atoms, as observed in Figs. 5 (b & c). The direction and the degree of spatial hybridization, manifested as the field lobe overlap, are observed for both electric and magnetic fields.

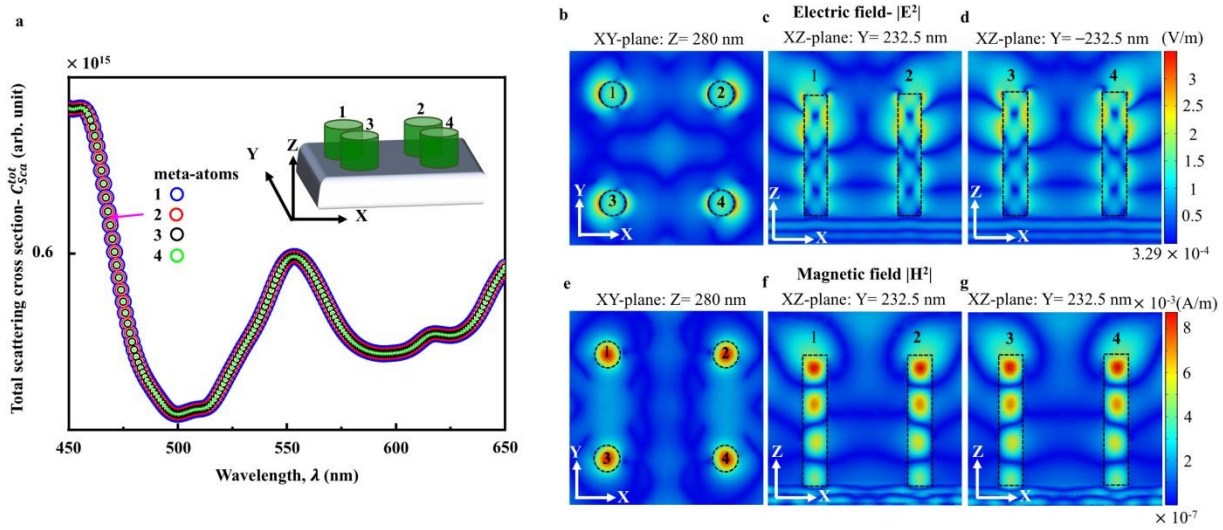

Fig. 5: a Total scattering cross-section (C_{sca}) EM spectrum of 4 (2 × 2) meta-atoms unit cell; Electric field distribution- b XY-Plane, Z=280 nm, c XZ-Plane, Y=232.5 nm, d XZ-Plane, Y=-232.5 nm; Magnetic field distribution- e XY-Plane, Z=280 nm, f XZ-Plane, Y=232.5 nm, g XZ-Plane, Y=-232.5 nm.

The asymmetry and inhomogeneity in the field distribution for each meta-atom are retained even on increasing the number of meta-atoms to 9 (3×3). The meta-atom (index-5), located in the centre of the metasurface, shows maximum localization of EM fields for the optimal periodicity regime $P_{MS} \sim \lambda_{MA-Res} \sim 465\ nm$, due to spatial hybridization with the fields of neighbouring meta-atoms across all directions, reflected as the field lobe overlap ($|H|^2$), as shown in Figs. 6 (g & m). This is why the total scattering cross section (C_{sca}^{total}) for the meta-atom (index-5) is also found to be maximum (Fig. 6b)[72,73]. The scattering cross-section as well as field distributions of each meta-atom, except the symmetrically surrounded centre one (index-5), are found to be different (Fig. 6), due to spatial hybridization with asymmetrically arranged neighbouring meta-atoms.

View Article Online
DOI: 10.1039/D6NA00100A

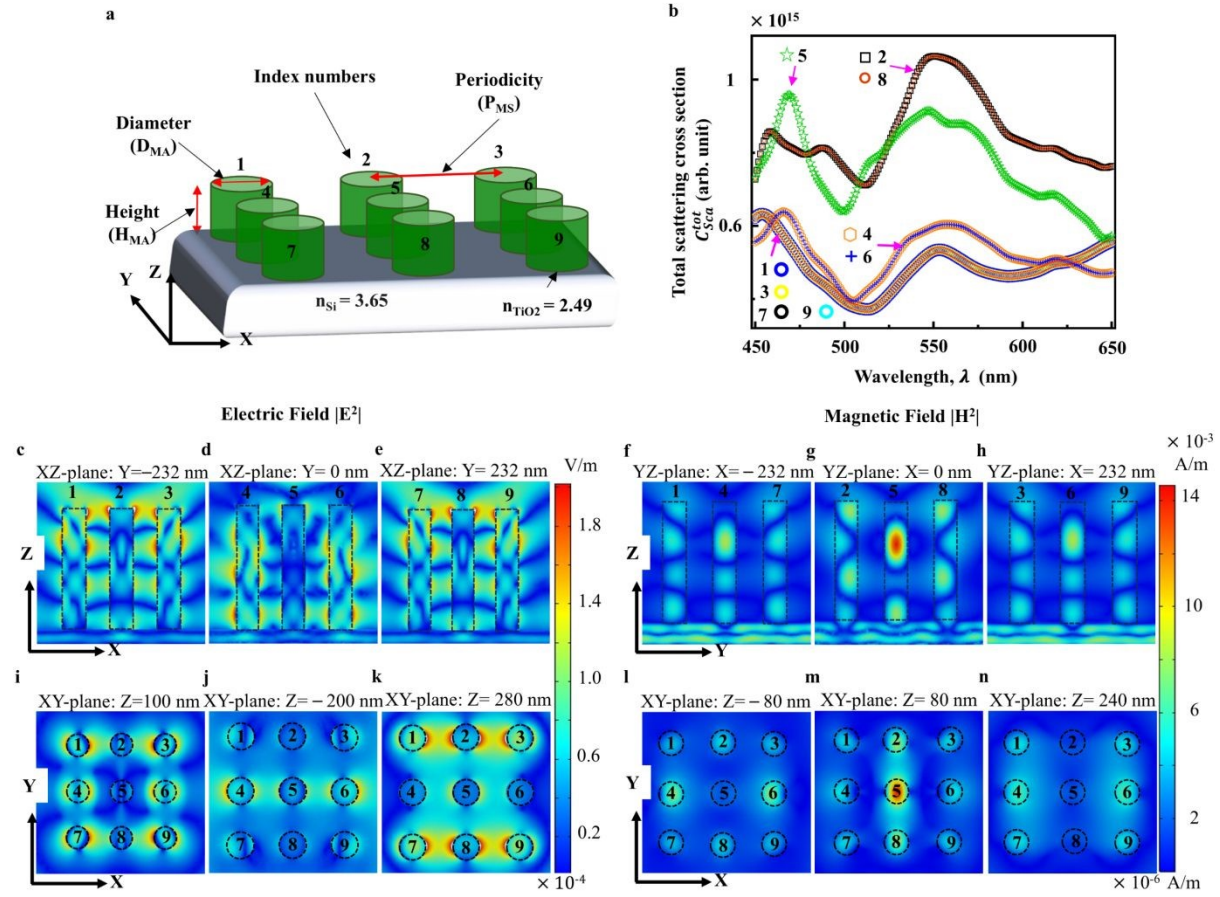

Fig. 6: a Schematic of 9 (3 × 3) meta-atoms metasurface, **b** Total scattering cross-section (C_{sca}) EM spectra, Electric field distribution- **c** XZ-Plane; Y=233.5 nm, **d** XZ-Plane; Y=0 nm, **e** XZ-Plane; Y= –232.5 nm, **i** XY-Plane; Z=100 nm, **j** XY-Plane; Z= –200 nm, **k** XY-Plane; Z=280 nm, Magnetic field distribution- **f** YZ-Plane; X= –233.5 nm, **g** YZ-Plane; X=0 nm, **h** YZ-Plane; X= 232.5 nm, **l** XY-Plane; Z= –80 nm, **m** XY-Plane; Z= 80 nm, **n** XY-Plane; Z=240 nm.

Conclusion

In conclusion, we have developed a bottom-up, comprehensive design framework for all-dielectric metasurface, to maximize resonance strength, manifested through enhanced scattering cross section and local field distribution, by controlled multipoles excitation, overlap, leading to controlled coupling among different resonance types- Mie, lattice, Rayleigh anomaly, on using geometric dimensions- height, diameter, lattice periodicity and number of meta-atoms as the control parameters, based on finite element method (FEM) numerical simulation. Spectral overlapping of all the four resonantly excited multipoles are demonstrated in a meta-atom on increasing the height beyond excitation wavelength. Lattice periodicity plays key role in determining the Q factor and spectral position of collective metasurface resonances, across different periodicity regimes with regard to Mie resonance wavelength. Two noteworthy aspects are found for the for the meta-atom spacing, the lattice periodicity regime ($P_{MS} \sim \lambda_{MA-Res}$). First, high Q factor is realized for the lattice periodicity regime ($P_{MS} \sim \lambda_{MA-Res}$), originating from maximum coupling of resonantly excited meta-atom multipole induced Mie resonances (λ_{MA-Res}) with lattice resonances (λ_{LS-Res}). Secondly, the resulting metasurface resonance wavelength

View Article Online
DOI: 10.1039/D6NA00100A

(λ_{MS-Res}) exactly coincides with the Rayleigh anomaly wavelength (λ_{RA}), which signifies maximum contribution from both –(a) lattice periodicity-controlled diffraction lattice resonances and (b) coupling of meta-atom Mie resonances with lattice resonances. However, for other lattice periodicity regimes ($P_{MS} < \lambda_{MA-Res}\ and\ P_{MS} > \lambda_{MA-Res}$), the coupling is found to be weak, leading to a decreased Q factor. In real world metasurfaces, consisting of finite number of meta-atoms, due to specific spatial arrangement of neighboring meta-atoms depending on the array size, spatial hybridization of EM field takes place, as manifested in the spectral resonance peak position tuning and local field asymmetry at sub meta-atom scale. Overall, the insights we presented not only enhance the basic understanding of multipole enhancement, overlap, and coupling among different resonance types, but also paves the way for practical design of metasurface photonics platforms with tailored light–matter interactions, applicable in areas including photonics quantum devices, resonant waveguide grating.

Acknowledgement
The author T.K.B. gratefully acknowledges the SRM Institute of Science and Technology, Kattankulathur, Chennai, India, for providing PhD fellowship. T.K.B. and J.M.L. express their sincere gratitude to Prof. Prabhakar Subrahmanyam, Prof. B. K. Gnanavel, Dr. Manikandan S for providing the high-performance computation facilities at the Center of Excellence for Electronic Cooling and Computational Fluid Dynamics (CFD), Département of Physics and Nanotechnology for High-Performance Computing Center (HPCC) at SRM Institute of Science and Technology, Kattankulathur, Chennai, India.

References

1 Z. A. Arnon, D. Pinotsi, M. Schmidt and S. Gilead, *ACS Applied Materials and Interfaces*, 2019, **10**, 20783–20789.
2 A. E. Seago, P. Brady, J. P. Vigneron and T. D. Schultz, *Journal of the Royal Society Interface*, 2009, **6**, S165-S184.
3 S. Kinoshita, S. Yoshioka and K. Kawagoe, *Proceedings of the Royal Society B: Biological Sciences*, 2002, **269**, 1417–1421.
4 González-Tudela, Alejandro, Andreas Reiserer, Juan José García-Ripoll, *Nature Reviews Physics*, 2024, **3**, 166–179.
5 S. Jahani and Z. Jacob, *Nature Nanotechnology*, 2016, **11**, 23–36.
6 M. Shehbaz, C. Du, D. Zhou, S. Xia and Z. Xu, *Applied Physics Reviews*, 2023, **10**, 1–45.
7 N. Meinzer, W. L. Barnes and I. R. Hooper, *Nature Photonics*, 2014, **8**, 889–898.
8 D. A. Powell, *Physical Review B - Condensed Matter and Materials Physics*, 2014, **90**, 1–10.
9 M. V. Rybin and Y. Kivshar, *NPJ Nanophotonics*, *NPJ Nanophotonics*, 2024, **1**, 43.
10 Y. Tamayama and K. Kanari, *Physical Review B*, 2020, **102**, 1–10.
11 W. Bogaerts, P. de Heyn, T. van Vaerenbergh, K. de Vos, S. Kumar Selvaraja, T. Claes, P. Dumon, P. Bienstman, D. van Thourhout and R. Baets, *Laser and Photonics Reviews*, 2012, **6**, 47–73.
12 A. Chiasera, Y. Dumeige, P. Féron, M. Ferrari, Y. Jestin, G. N. Conti, S. Pelli, S. Soria and G. C. Righini, *Laser and Photonics Reviews*, 2010, **4**, 457–482.
13 J. D. Joannopoulos, P. R. Villeneuve and S. Fan, *Nature*, 1997, **386**, 143–149.
14 Y. Kivshar, *Nano Letters*, 2022, **22**, 3513–3515.
15 V. E. Babicheva and Andrey B. Evlyukhin, *Advances in Optics and Photonics*, 2023, **16**,

View Article Online
DOI: 10.1039/D6NA00100A

539–658.
16 A. Vaskin, R. Kolkowski, A. F. Koenderink and I. Staude, *Nanophotonics*, 2019, **8**, 1151–1198.
17 Y. L. Tang, T. H. Yen, K. Nishida, C. H. Li, Y. C. Chen, T. Zhang, C. K. Pai, K. P. Chen, X. Li, J. Takahara and S. W. Chu, *Nature Communications*, 2023, **14**, 1–8.
18 L. Huang, R. Jin, C. Zhou, G. Li, L. Xu, A. Overvig, F. Deng, X. Chen, W. Lu, A. Alù and A. E. Miroshnichenko, *Nature Communications*, 2023, **14**, 1–9.
19 G. Quaranta, G. Basset, O. J. F. Martin and B. Gallinet, *Laser and Photonics Reviews*, 2018, **12**, 1–31.
20 M. F. Limonov, M. V. Rybin, A. N. Poddubny and Y. S. Kivshar, *Nature Photonics*, 2017, **11**, 543–554.
21 S. Tsoi, F. J. Bezares, A. Giles, J. P. Long, O. J. Glembocki, J. D. Caldwell and J. Owrutsky, *Applied Physics Letters*, 2016, **108**, 111101.
22 S. Baur, S. Sanders and A. Manjavacas, *ACS Nano*, 2018, **12**, 1618–1629.
23 S. Shen, Z. Ruan, S. Li, Y. Yuan and H. Tan, *Results in Physics*, 2021, **23**, 104057.
24 H. Radhakrishnan, T. K. Basha, J. M. Laskar, G. Krishnan, S. Dhara and R. Pandian, *ACS Photonics*, 2025, **12**, 4503–4511.
25 C. W. Hsu, B. Zhen, A. D. Stone, J. D. Joannopoulos and M. Soljacic, *Nature Reviews Materials*, 2016, **1**, 16048.
26 T. Liu, R. Xu, P. Yu, Z. Wang and J. Takahara, *Nanophotonics*, 2020, **9**, 1115–1137.
27 J. M. Laskar, J. Philip and B. Raj, *Physical Review E - Statistical, Nonlinear, and Soft Matter Physics*, 2008, **78**, 1–9.
28 V. Zubyuk, L. Carletti, M. Shcherbakov and S. Kruk, *APL Materials*, 2021, **9**, 060701.
29 S. A. Schulz, et. al., *Applied Physics Letters*, 2024, **124**, 1–114.
30 Z. Zhang, P. Liu, W. Lu, P. Bai, B. Zhang, Z. Chen, S. A. Maier, J. Gómez Rivas, S. Wang and X. Li, *Fundamental Research*, 2023, **3**, 822–830.
31 G. W. Castellanos, P. Bai and J. Gómez Rivas, *Journal of Applied Physics*, 2019, **125**, 213105.
32 V. E. Babicheva and J. V. Moloney, *Nanophotonics*, 2018, **7**, 1663–1668.
33 V. I. Zakomirnyi, A. E. Ershov, V. S. Gerasimov, S. V. Karpov, H. Ågren and I. L. Rasskazov, *Optics Letters*, 2019, **44**, 5743.
34 C. H. Palmer and F. C. Evering, *Journal of the Optical Society of America*, 1964, **54**, 844.
35 R. W. Wood, *Proceedings of the Physical Society of London*, 1901, **18**, 269–275.
36 Lord Rayleigh, *Proceedings of the Royal Society of London*, 1907, **79**, 399–416.
37 V. E. Babicheva and A. B. Evlyukhin, *Laser and Photonics Reviews*, 2017, **11**, 1–10.
38 A. Han, C. Dineen, V. E. Babicheva and J. V. Moloney, *Nanophotonics*, 2020, **9**, 3545–3556.
39 R. Xu and J. Takahara, *Optics Letters*, 2021, **46**, 3596.
40 C. Liu, H. Ye, Y. Wang, Y. Sun, Y. Liu, Z. Yu and L. Yu, *Optics Letters*, 2020, **45**, 4847.
41 V. E. Babicheva and A. B. Evlyukhin, *ACS Photonics*, 2018, **5**, 2022–2033.
42 K. Sakai, K. Nomura, T. Yamamoto, T. Omura and K. Sasaki, *Scientific Reports*, 2016, **6**, 1–7.
43 D. Hähnel, C. Golla, M. Albert, T. Zentgraf, V. Myroshnychenko, J. Förstner and C. Meier, *Light: Science and Applications*, 2023, **12**, 23–26.
44 T. X. Hoang, D. Leykam, H. S. Chu, C. E. Png, F. J. García-Vidal and Y. S. Kivshar, *Physical Review Research*, 2025, **7**, 13316.
45 Bulgakov, Evgeny N., and Almas F. Sadreev, *Physical Review A*, 2019, **3**, 033851.

View Article Online
DOI: 10.1039/D6NA00100A

46 Z. Liu, Y. Xu, Y. Lin, J. Xiang, T. Feng, Q. Cao, J. Li, S. Lan and J. Liu, *Physical Review Letters*, 2019, **123**, 1–6.
47 V. Karimi and V. E. Babicheva, *Optics Express*, 2023, **31**, 16857.
48 S. Liu, A. Vaskin, S. Campione, O. Wolf, M. B. Sinclair, J. Reno, G. A. Keeler, I. Staude and I. Brener, *Nano Letters*, 2017, **17**, 4297–4303.
49 J. Ma, J. Zhang, J. Horder, A. A. Sukhorukov, M. Toth, D. N. Neshev and I. Aharonovich, *Advanced Materials*, 2024, **36**, 1–15.
50 S. Izadshenas and K. Słowik, *APL Materials*, 2023, **11**, 1–9.
51 T. C. Ellis, S. Eslami and S. Palomba, *Nanophotonics*, 2024, **13**, 2707–2739.
52 L. Huang, L. Xu, M. Woolley and A. E. Miroshnichenko, *Advanced Quantum Technologies*, 2020, **3**, 1900126.
53 J. R. DeVore, *Journal of the Optical Society of America*, 1951, **41**, 416.
54 D. E. Aspnes and A. A. Studna, *Physical Review B*, 1983, **27**, 985–1009.
55 R. Alaee, C. Rockstuhl and I. Fernandez-Corbaton, *Optics Communications*, 2018, **407**, 17–21.
56 M. V. Rybin, K. L. Koshelev, Z. F. Sadrieva, K. B. Samusev, A. A. Bogdanov, M. F. Limonov and Y. S. Kivshar, *Physical Review Letters*, 2017, **119**, 1–5.
57 I. Staude, A. E. Miroshnichenko, M. Decker, N. T. Fofang, S. Liu, E. Gonzales, J. Dominguez, T. S. Luk, D. N. Neshev, I. Brener and Y. Kivshar, *ACS Nano*, 2013, **7**, 7824–7832.
58 J. van de Groep and A. Polman, *Optics Express*, 2013, **21**, 26285.
59 C. Liu, L. Chen, T. Wu, Y. Liu, R. Ma, J. Li, Z. Yu, H. Ye and L. Yu, *New Journal of Physics*, 2020, **22**, 023018.
60 R. Alaee, R. Filter, D. Lehr, F. Lederer and C. Rockstuhl, *Optics Letters*, 2015, **40**, 2645.
61 A. Radkovskaya, S. Kiriushechkina, A. Vakulenko, P. Petrov, L. Solymar, L. Li, A. Vallecchi, C. J. Stevens and E. Shamonina, *Journal of Applied Physics*, 2018, **124**, 104901.
62 J. Hou, X. Zhang, Y. Guo, R. Z. Zhang and M. Guo, *Scientific Reports*, 2023, **13**, 1–7.
63 V. E. Babicheva and A. B. Evlyukhin, *Journal of Applied Physics*, 2021, **129**, 040402.
64 D. Visser, D. Y. Chen, Y. Désières, A. P. Ravishankar and S. Anand, *Scientific Reports*, 2020, **10**, 12527.
65 F. J. G. De Abajo, *Reviews of Modern Physics*, 2007, **79**, 1267–1290.
66 M. Decker, I. Staude, M. Falkner, J. Dominguez, D. N. Neshev, I. Brener, T. Pertsch and Y. S. Kivshar, *Advanced Optical Materials*, 2015, **3**, 813–820.
67 W. Liu and Y. S. Kivshar, *Optics Express*, 2018, **26**, 13085.
68 S. Izadshenas and K. Słowik, *APL Materials*, 2023, **11**, 081120.
69 S. Sehrawat, R. Kolkowski and A. Shevchenko, *New Journal of Physics*, 2024, **26**, 23050.
70 I. Allayarov, A. B. Evlyukhin and A. Calà Lesina, *Optics Express*, 2024, **32**, 5641.
71 M. Pascale, G. Miano, R. Tricarico and C. Forestiere, *Scientific Reports*, 2019, **9**, 1–21.
72 Y. Guo, Y. Liao, Y. Yu, Y. Shi and S. Xiong, *Optics Letters*, 2020, **45**, 5604.
73 N. Ustimenko, C. Rockstuhl and A. B. Evlyukhin, *Physical Review B*, 2024, **109**, 1–14.

View Article Online
DOI: 10.1039/D6NA00100A

Data Availability:

Owing to their large size, the numerical computational simulation files could not be uploaded. Nevertheless, the associated data are available from the corresponding author upon request.